Journal of Materials Science and Chemical Engineering, 2026, 14(11), 133-150
https://www.scirp.org/journal/msce
ISSN Online: 2327-6053
ISSN Print: 2327-6045

An Integrated Statistical Framework for Evaluating Mechanical Durability and Lifecycle Performance of Photovoltaic Backsheets

Joseph Moses*, Tridip K. Bardhan

Department of Industrial, Mechatronics, and Systems Engineering, Morgan State University, Baltimore, Maryland, USA
Email: *jomos6@morgan.edu

How to cite this paper: Moses, J. and Bardhan, T.K. (2026) An Integrated Statistical Framework for Evaluating Mechanical Durability and Lifecycle Performance of Photovoltaic Backsheets. *Journal of Materials Science and Chemical Engineering*, **14**, 133-150.
https://doi.org/10.4236/msce.2026.1411009

Received: September 24, 2026
Accepted: November 24, 2026
Published: November 27, 2026

Copyright © 2026 by author(s) and Scientific Research Publishing Inc.
This work is licensed under the Creative Commons Attribution International License (CC BY 4.0).
http://creativecommons.org/licenses/by/4.0/
Open Access

Abstract

Photovoltaic (PV) backsheets are subjected to continuous environmental stressors, resulting in gradual tensile strength degradation and reduced long-term module reliability. This paper presents a six-stage statistical modeling framework to quantify how cumulative ultraviolet (UV) exposure, temperature, relative humidity, and wind speed each contribute to tensile strength loss in a multilayer PPE-based PV backsheet (polyethylene terephthalate/polyethylene terephthalate/ethylene vinyl acetate, PET/PET/EVA). Pearson correlation using a field dataset of 511 sequential observations of cumulative UV doses (0.84 MJ/m^2 to 271.6 MJ/m^2) established UV irradiance as the most important degradation driver ($r = -0.960$, $R^2 = 0.921$). Since the observations constitute one degradation time series, the serial autocorrelation was checked with the Durbin-Watson statistic and confirmed, necessitating Newey-West heteroscedasticity and autocorrelation-consistent (HAC) standard errors in all the inferential tests. Following a HAC correction, cumulative UV is the strongest predictor. The rate of tensile strength degradation with respect to cumulative UV exposure was estimated at 0.21 - 0.22 MPa per MJ/m^2, based on ordinary least squares (OLS), multiple regression, and weighted least squares (WLS) models applied following the Breusch-Pagan test for heteroscedasticity. The second-order regression model gave a better predictive performance with $R^2 = 0.9686$ and RMSE = 3.033 MPa; six of the nine higher-order terms were found significant after HAC correction, whereas the UV Temperature interaction became insignificant, which demonstrates the practical effect of the autocorrelation correction. Weibull distribution fitting was the best performer, with shape parameter $\beta = 15.87$ and B_{10} tensile strength threshold of 193.14 MPa at approximately 15.4 years of field exposure. Cost benefit analysis showed that premium fluoropolymer backsheets had a net present value benefit of about $7.55 per module in comparison to 25-year de-

sign life. These results provide a model of PV backsheet degradation, which can be easily reproduced, and which can be directly applied to reliability-based design and cost-effective lifecycle models.

Keywords

Photovoltaic Backsheet, Tensile Strength Degradation, Second-Order Polynomial Regression, Weighted Least Squares, Newey-West HAC, Serial Autocorrelation, Weibull Reliability, UV Exposure

1. Introduction

Having a photovoltaic module to work consistently over 25 to 30 years is not merely an engineering dream, it is a guarantee that is required by the contract in most project financiers [1] [2]. The backsheet is often not given serious consideration as one of the elements with the highest long-term mechanical risk. It has three functions, to conduct electrical protection against high-voltage fields, to provide mechanical protection to the interior cell assembly, and to provide a moisture and chemical barrier at the exposed rear side of the module. Once the backsheet starts to degenerate, the module will also degenerate, and the degeneration process is usually irreversible.

The laminate type of PPE is built by applying a white-colored polyethylene terephthalate (WPET) outermost layer on the cell side, clear polyethylene terephthalate (PET) core, and EVA inner layer at the interface with the air. The three-layered structure is commercially common due to the mechanical support that is offered by PET: tensile strength, dimensional stability, and breakdown at electricity [3] [4]. The EVA coating guarantees compliance of adhesive with the module encapsulant. Both are degraded in ultraviolet light, facilitating the chain scission and carbonyl group formation in the polymer backbone and steadily reducing the tensile strength and encouraging surface cracking [5] [6].

The cumulative UV irradiance is the most common driver of mechanical degradation in PET-based backsheets, followed by the temperature and relative humidity as secondary stressors, which interact with each other [3] [4]. The technical difficulty of converting such a qualitative insight into a validated quantitative model is more challenging than it may seem since multilayer degradation is spatially heterogeneous, the relationships between stressors and responses are nonlinear and interactive, and the measurement variance increases with the accumulation of UV [7] [8].

The predictive accuracy is not enough from an industrial and systems engineering perspective. The model must also be statistically defensible: violations fixed, and inference made with reasonable grounds. Second-order polynomial regression is effectively proven to describe the primary effects and an interaction between multiple environmental factors [9]. Two statistical complications are addressed directly in this paper. First, the OLS residuals are tested using the Breusch-

Pagan test which identifies heteroscedasticity and then is corrected using the weighted least squares (WLS). Second, and more importantly, the 511 observations are obtained in one sequence of degradation trace, but not measurements of several specimens. The Durbin-Watson statistic is thus used to test serial autocorrelation and correct the whole procedure with Newey-West HAC standard errors [10], that deal with both conditions of heteroscedasticity and autocorrelation and give valid results in either scenario. The degradation model is then converted into practical estimates of failure probability through statistical reliability analysis [11] [12].

These are the six stages of the analysis through which this paper makes its contribution: 1) Pearson correlation to rank the importance of stressors; 2) OLS regression with full ANOVA; 3) Breusch-Pagan and Durbin-Watson testing with WLS and Newey-West HAC corrections; 4) the second-order regression of the nonlinear and interaction effects and HAC corrected inference; 5) Weibull versus lognormal distribution comparison by AIC, BIC, and KS; and 6) a cost benefit analysis with a discounted payoff using a 25-year design horizon comparing the premium strategy and the standard backsheet strategy.

2. Literature Review

2.1. Mechanical Degradation of PV Backsheet Polymers

Tensile strength is the most operationally relevant mechanical property to determine the reliability of backsheet since it defines the limit between the laminates that can support field loads and those that cannot [6] [13]. The location of this threshold depends on the exact composition of the layer and history of its processing, which is also supported by mechanical characterization research of PV encapsulation polymers [14]. Three intersecting degradation pathways (photo-oxidation of UV, chain scission through moisture, and crystallization in amorphous domains of polymer under heat) diminish tensile strength due to outdoor exposure [3] [4].

One of the most detailed descriptions of such degradation process in commercial PPE backsheets has been provided by Lin *et al.* [3], who combined 510 days of outdoor aging at Gaithersburg, Maryland, and NIST SPHERE accelerated laboratory exposure. Tensile strength and break elongation reduced by 26.7% during the same period and surface cracking appeared between days 125 and 184. Tests of mode I fracture toughness (K_{Ic}) gave a value of 0.03 to 0.12 MPa·m$^{1/2}$ on tests of channel-cracking fragmentation on WPET outer layer, which is significantly lower than the 4.5 to 5.5 MPa·m$^{1/2}$ in tests of unaged PET. Notably, the experiment revealed that rapid exposure to UV (acceleration) recapitulated the patterns of the field damage, thus approving cumulative UV dose to serve as a useful proxy of a field exposure time in a sequence of degradation records.

Lyu *et al.* [1] used the field data of multiple sites to verify that UV irradiance always makes a prevailing difference when predicting mechanical property degradation in various climatic areas. Mitterhofer *et al.* [7] have performed a hybrid of

finite-element simulation and fragmentation testing and concluded that the severity of the crack in AAA and PPE backsheets is strongly dependent on the properties of the adhesive layer at the interfaces of PET. Smith *et al.* [8] applied this observation to bifacial transparent backsheets and showed that the composition of the layers allows controlling the degree to which UV-induced chemical damages infiltrate the PET core.

2.2. Statistical and Predictive Modeling Approaches

The regression-based models have been traditionally used as the main analytical system of measuring the correlation between environmental stressors and the performance of the PV components. Lyu *et al.* [1] demonstrated that the ratio of the variability in degradation of mechanical property was higher with UV dose than with temperature or humidity in several field sites. Lyu *et al.* [1] utilized regression methods to field-exposed backsheets and proved that it can reliably predict chemical and mechanical degradation results based on their exposure history.

The second-order polynomial regression model builds on the linear model, adding squared and cross-product interaction terms to the model, and it can account for nonlinear and synergistic stressor effects that are typical of polymer aging data [9]. As shown by Damo *et al.* [5], this method was found useful in predicting multi-factor degradation of PVs under Arrhenius-type degradation conditions, showing that the synergies present between stressors were better represented by non-linear specifications that were not identified in purely linear ones. Interpretable parametric regression models are still the favored technique in degradation science when the physics of the problem limits the functional form and the cause-and-effect information about individual stress factors is needed.

Although it is popular, two statistical complications, namely heteroscedasticity and the serial autocorrelation, do not receive adequate research in PV backsheet regression. Heteroscedasticity, which is a situation where the exposure variable increases the amount of residual variance, inflates t-statistic and suppresses confidence intervals [15]. Serial autocorrelation also exaggerates conventional t -statistics when observations are ordered serially on a single specimen since successive residual values do not have a known microstructural state. Newey-West heteroskedasticity-and-autocorrelation consistent (HAC) standard errors simultaneously control both offenses, and they are the correction of choice in situations of heteroscedasticity and autocorrelation [15].

2.3. Reliability Modeling of PV Backsheets

The reliability modeling tool of interest is known as Weibull analysis, which is suitable for assessing the lifetime of PV components and field studies have proved that it is suitable in a variety of climatic zones [2] [16]. Its shape parameter β is particularly useful: values above 1 describe a wear-out process where the hazard rate rises over time, which is physically consistent with cumulative UV-driven polymer chain scission. Shape parameters were reported to range between 2 and

20 and this was a degradation mode of wear-out of modules installed in Australian climates [16]. Conversely, lognormal distribution is set to offer a correct fit to multiplicative failure processes in which every degradation step enhances the previous one [17]. Al Mahdi *et al.* [2] found tensile strength degradation and surface cracking as the most common mechanical failure modes of backsheets made of polymer and noted that Weibull based reliability modeling directly relates to maintenance scheduling and warranty design.

2.4. Gaps in Literature

Three gaps in the published literature motivated this work. First, backsheet regression analyses rarely test the heteroscedasticity or serial autocorrelation model thus making the validity of reported standard errors and p-values questionable, especially with single-specimen degradation data. Second, direct comparisons on the basis of AIC/BIC between Weibull and lognormal distributions on the basis of actual data on field-scale tensile strength usage are uncommon; hence, the best distribution to describe PPE backsheets is not empirically determined. Third, there is still no unified framework that combines the second-order predictive modeling of degradation and reliability distribution fitness with cost-benefit analysis based on net present value (NPV) to this type of material. The current study takes care of all three shortcomings.

3. Methodology

3.1. Material and Dataset Description

The backsheet under study of this research is a multilayer polymer laminate of PPE-type, which consists of a white-pigmented polyethylene terephthalate (WPET) layer on the cell side, a clear PET core layer, and an ethylene-vinyl acetate (EVA) layer on the air-side face. Any tensile testing was performed on samples that resembled the entire multilayer laminate, thus the tenacity strength values obtained were a response of load bearing of the PET/PET/EVA assembly as a whole and not any layer.

The data set has 511 concurrent field measurements of tensile strength (MPa) and temperature (T, ˚C), relative humidity (RH, %), wind speed (WS, m/s), and cumulative dose of UV irradiance (UV_{cum}, MJ/m^2). The cumulative UV irradiance varies in a linear increasing fashion from 0.84 MJ/m^2 to 271.6 MJ/m^2 over the duration of the record; this is equivalent to the history of continued field exposure of a single specimen. This monotonic form places the data as a degradation time series in lieu of a cross-sectional sample which has direct implications on testing autocorrelation under discussion in Section 3.4. **Table 1** shows descriptive statistics.

3.2. Pearson Correlation Analysis

Pearson correlation coefficients were computed between each environmental stressor and tensile strength to characterize the direction and linear strength of each association. The bivariate R^2 provided a first estimate of individual stressor importance and informed variable selection for subsequent regression modeling.

Table 1. Descriptive statistics for the 511-observation field dataset.

Variable	n	Min	Max	Mean	Std Dev	Median
Temperature (˚C)	511	−13.84	28.74	14.05	10.46	17.87
Relative Humidity (%)	511	49.18	100.00	78.92	10.03	79.29
Wind Speed (m/s)	511	0.76	7.28	2.15	0.88	1.98
Cumul. UV (MJ/m^2)	511	0.84	271.6	133.7	72.9	126.7
Tensile Strength (MPa)	511	168.76	241.93	215.15	17.14	213.73

3.3. Multiple Linear Regression and ANOVA

Multiple linear regression modeled tensile strength as a function of all four stressors simultaneously. The OLS regression model is:

$$\mathrm{TS} = \beta_0 + \beta_1 \mathrm{UV}_{\mathrm{cum}} + \beta_2 T + \beta_3 \mathrm{RH} + \beta_4 \mathrm{WS} + \varepsilon \tag{1}$$

where TS is tensile strength in MPa, $\mathrm{UV}_{\mathrm{cum}}$ is cumulative UV dose in MJ/m^2, T is temperature in ˚C, RH is relative humidity in %, WS is wind speed in m/s, β_i are regression coefficients, and ε is the error term. Model significance was assessed by ANOVA at $\alpha = 0.05$. Goodness-of-fit was measured by R^2, adjusted R^2, and RMSE.

3.4. Autocorrelation and Heteroscedasticity Testing with HAC Correction

Because the 511 observations form a single specimen's sequential degradation record, two violations were anticipated and formally tested. Both tests were applied before any inferential conclusions were drawn from the regression output.

Heteroscedasticity was tested using the Breusch-Pagan Lagrange Multiplier test. The test statistic LM = $n \times R^2_{\mathrm{BP}}$ follows a chi-squared distribution with degrees of freedom equal to the number of predictors. Where heteroscedasticity was confirmed, a WLS model was developed with weights $w_i = \left(\mathrm{UV}_{\mathrm{cum},i} + 1\right)^{-\gamma}$, where the variance exponent γ was estimated by regressing $\log\left(e_i^2\right)$ on $\log\left(\mathrm{UV}_{\mathrm{cum},i}\right)$.

Serial autocorrelation was tested using the Durbin-Watson statistic

$$\mathrm{DW} = \frac{\sum_{i=2}^{n}\left(e_i - e_{i-1}\right)^2}{\sum_{i=1}^{n} e_i^2},$$

where values near 2 indicate no autocorrelation and values well below 2 indicate positive autocorrelation. For a single-specimen degradation record with monotonically increasing cumulative UV, positive residual autocorrelation is expected: each observation inherits the specimen's current microstructural damage state from the previous one. The Ljung-Box Q (1) test was applied alongside DW to confirm the direction and strength of the serial dependence.

Where both violations were present, Newey-West HAC standard errors were applied to all regression models. HAC standard errors use a Bartlett kernel-weighted sandwich estimator to produce valid inference under simultaneous heteroscedasticity and autocorrelation [15]. Bandwidth was set by $h = \left\lfloor 4\left(\frac{n}{100}\right)^{2/9} \right\rfloor = 5$. OLS and

WLS coefficient estimates are unbiased under autocorrelation and remain unchanged; only the standard errors and derived test statistics are corrected. Figure 1 shows OLS residual diagnostics; Figure 2 shows the WLS residual comparison.

3.5. Second-Order Polynomial Regression Model

A second-order polynomial regression model was developed to capture quadratic and interaction effects among the stressors, following the polynomial modeling framework in Chen *et al.* [9]. Wind speed was excluded from the polynomial model: its Pearson correlation was negligible (r = +0.065) and its OLS coefficient was non-significant even before HAC correction (t = 1.17, p = 0.243). The retained stressors were UV_{cum}, temperature, and relative humidity:

$$\begin{aligned} \mathrm{TS} = {} & \beta_0 + \beta_1 \mathrm{UV} + \beta_2 T + \beta_3 \mathrm{RH} + \beta_4 \mathrm{UV}^2 + \beta_5 T^2 + \beta_6 \mathrm{RH}^2 \\ & + \beta_7 (\mathrm{UV} \times T) + \beta_8 (\mathrm{UV} \times \mathrm{RH}) + \beta_9 (T \times \mathrm{RH}) + \varepsilon \end{aligned} \tag{2}$$

Parameters were estimated by OLS. All standard errors are Newey-West HAC-corrected. Non-significant main effects were retained where their interaction or quadratic terms were significant, following the effect-heredity principle. Specifically, the non-significant linear Temperature and RH main effects were retained because their quadratic and interaction terms (T^2, $T \times$ RH, RH^2, UV × RH) are statistically significant after HAC correction. Term significance was assessed at α = 0.05 using HAC-corrected t-statistics. Figure 3 shows fitted-value contour plots for the two interactions that remained significant after HAC correction.

3.6. Reliability Analysis: Weibull and Lognormal Distributions

Two distributions were fitted to the tensile strength data by maximum likelihood estimation. The two-parameter Weibull probability density function is [17]:

$$f(x;\beta,\eta) = \frac{\beta}{\eta}\left(\frac{x}{\eta}\right)^{\beta-1} \exp\left[-\left(\frac{x}{\eta}\right)^{\beta}\right], \quad x > 0 \tag{3}$$

where $\beta > 0$ is the shape parameter, $\eta > 0$ is the scale parameter, and x denotes tensile strength in MPa. The corresponding reliability function is $R(x) = \exp\left[-\left(\frac{x}{\eta}\right)^{\beta}\right]$.

The lognormal probability density function is [17]:

$$f(x;\mu,\sigma) = \frac{1}{x\sigma\sqrt{2\pi}} \exp\left[-\frac{(\ln x - \mu)^2}{2\sigma^2}\right], \quad x > 0 \tag{4}$$

where x is tensile strength in MPa, and μ and σ are the log-scale location and scale parameters. Model selection used $\mathrm{AIC} = 2k - 2L$ (where L is the maximized log-likelihood and k the number of parameters), $\mathrm{BIC} = k \cdot \ln(n) - 2L$, and the Kolmogorov-Smirnov statistic. The standard KS critical value for known parameters at n = 511 and α = 0.05 is $1.358/\sqrt{511} \approx 0.060$. Because parameters were estimated from the data, the Li [18] modified threshold of $0.895/\sqrt{511} \approx 0.040$ is the relevant benchmark, and KS is used as a relative diagnostic rather than a standalone pass/fail test. Figure 4 shows both probability plots.

The B_{10} threshold used here is the 10th percentile of the fitted tensile strength distribution, meaning the strength value below which 10% of the statistical population falls under the model. This is a strength-based reliability criterion, distinct from the conventional time-to-failure B_{10} life. The cumulative UV dose at which the population-mean predicted tensile strength reaches the B_{10} threshold is obtained by inverting the OLS regression equation (Equation (1)) with temperature, relative humidity, and wind speed held at their dataset means (14.05˚C, 78.92%, and 2.15 m/s, respectively). Conversion to an estimated service life uses a reference UV accumulation rate of 15 MJ/m^2/year for mid-latitude temperate US conditions [4]. Sites with different irradiance levels should substitute local values.

3.7. Cost-Benefit Analysis

A discounted cost-benefit analysis compared standard PPE and premium fluoropolymer backsheet strategies over a 25-year module design life. Total cost follows the TC = FC + VC framework. Initial costs are $25/module (standard PPE) and $55/module (premium fluoropolymer), from PV bill-of-materials data [19] [20]. The total field replacement cost of $92/module, covering material, de-mounting, re-lamination, reinstallation, and downtime, draws on O&M benchmarks from Lawrence Berkeley National Laboratory [21]. A 6% annual discount rate was applied [20], with the standard backsheet replacement cycle set at 15.4 years from the Weibull B_{10} result, giving NPV = $92/$(1.06)^{15.4}$ = $37.55 per module. Break-even was solved as: the premium strategy is favored when undiscounted replacement cost exceeds $30 × $(1.06)^{15.4}$ ≈ $74/module.

4. Results

4.1. Pearson Correlation Analysis

Cumulative UV irradiance correlated with tensile strength at $r = -0.960$ (R^2 = 0.921, $p < 0.001$), accounting for 92.1% of total variance on its own. Temperature ($r = -0.040$), relative humidity ($r = +0.143$), and wind speed ($r = +0.065$) each showed negligible to weak individual associations. Results are in Table 2.

Table 2. Pearson correlation coefficients between environmental stressors and tensile strength ($n = 511$).

Environmental Stressor	r (Pearson)	R^2	Interpretation
Cumulative UV (MJ/m^2)	−0.960	0.921	Dominant driver
Temperature (˚C)	−0.040	0.002	Negligible
Relative Humidity (%)	+0.143	0.020	Weak positive
Wind Speed (m/s)	+0.065	0.004	Negligible

UV absorption in PET drives Norrish-type chain scission at carbonyl ester bonds, producing chromophoric oxidation products that steadily weaken the laminate [3] [6]. The positive humidity correlation ($r = +0.143$) is weak in isolation but does not rule out an interactive contribution: absorbed moisture can delay

brittle crack propagation at intermediate UV doses, while accelerating hydrolytic chain scission at higher doses [4]. Field studies in harsh multi-stressor climates confirm that interaction effects can account for substantial additional degradation beyond UV alone [22].

4.2. OLS Multiple Linear Regression and ANOVA

The OLS model explained 92.5% of total tensile strength variance (R^2 = 0.9249, RMSE = 4.715 MPa; F(4, 506) = 1557.90, p < 0.001). The fitted equation is:

$$\hat{TS} = 237.016 - 0.2245 \cdot UV_{cum} + 0.0034 \cdot T + 0.0927 \cdot RH + 0.3644 \cdot WS \quad (5)$$

The UV coefficient (β_1 = −0.2245 MPa per MJ/m^2) projects to a total tensile strength reduction of approximately 60.8 MPa across the observed UV range, or 25.1% of the initial value of 241.93 MPa. This sits close to the 26.7% reduction Lin *et al.* [3] measured experimentally under comparable outdoor conditions, providing external validation. The ANOVA decomposition is in Table 3; coefficient estimates are in Table 4 and Table 5.

Table 3. ANOVA table for OLS multiple linear regression model.

Source	SS	df	MS	F	p-value
Regression	138537.7	4	34634.4	1557.90	<0.001
Residual	11250.3	506	22.23	--	--
Total	149,788.0	510	--	--	--

Table 4. OLS coefficient estimates with standard OLS standard errors (R^2 = 0.9249, RMSE = 4.715 MPa).

Term	Coefficient	OLS Std Error	*t*	p-value
Intercept	237.016	3.142	75.43	< 0.001
UV_{tum} (MJ/m^2)	−0.2245	0.00402	−55.85	< 0.001
Temperature (˚C)	0.0034	0.0272	0.13	0.902
Relative Humidity (%)	0.0927	0.0284	3.26	0.001
Wind Speed (m/s)	0.3644	0.312	1.17	0.243

Table 5. OLS coefficient estimates with newey-west HAC standard errors (DW = 0.038, ρ_1 = 0.981; bandwidth h = 5; n = 511).

Term	Coefficient	HAC Std Error	*t* (HAC)	p (HAC)
Intercept	237.016	2.589	91.56	<0.001
UV_{tum} (MJ/m^2)	−0.2245	0.00867	−25.89	**<0.001**
Temperature (˚C)	0.0034	0.03182	0.11	0.914
Relative Humidity (%)	0.0927	0.03262	2.84	**0.005**
Wind Speed (m/s)	0.3644	0.24031	1.52	0.130

Coefficient estimates are identical to OLS; HAC correction changes only standard errors and derived statistics. Bold = HAC-significant (p < 0.05). UV_{tum} t-statistic falls from −55.85 (OLS) to −25.89 (HAC) but remains highly significant. RH retains significance (p = 0.005).

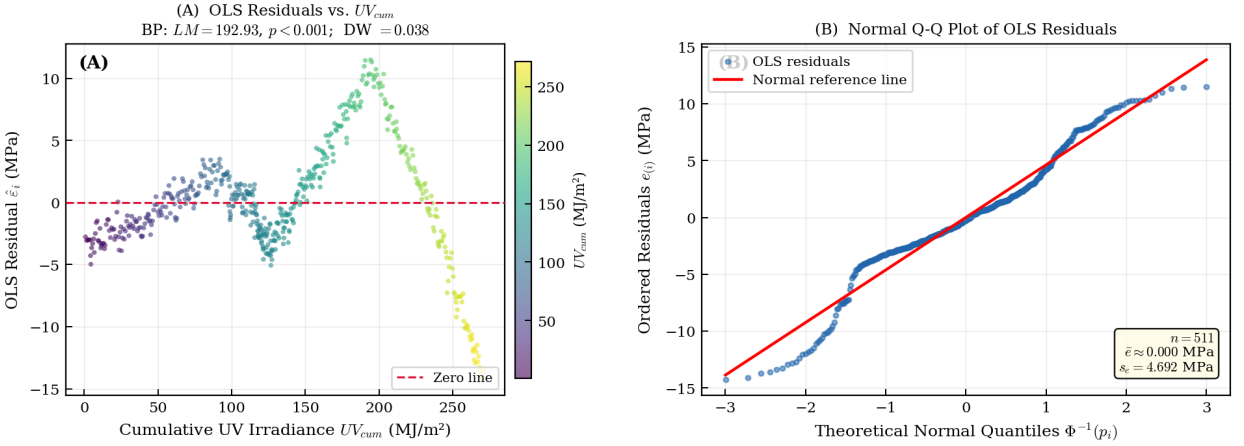

Figure 1. OLS residual diagnostics. Panel (A): residual spread widens markedly with increasing UV dose, confirming heteroscedasticity (BP LM = 192.93, p < 0.001) and autocorrelation (DW = 0.038). Panel (B): normal Q-Q plot of OLS residuals.

4.3. Autocorrelation Test Results and HAC Correction

The Durbin-Watson statistic for the OLS residuals was 0.038, far below the lower critical bound of approximately 1.82 for $n = 511$, $k = 4$ at $\alpha = 0.05$. The lag-1 residual autocorrelation was $\rho_1 = 0.981$, and the Ljung-Box Q (1) test confirmed the result decisively ($Q = 494.6$, p < 0.001). After fitting the polynomial model, which absorbs the primary systematic UV trend, the DW statistic improved only to 0.231 and the lag-1 autocorrelation remained at 0.884. Autocorrelation persisted because each observation carries forward the specimen's accumulated microstructural damage state from the preceding one, a form of temporal dependence that the regression model itself cannot remove.

The practical consequence is that the conventional OLS standard errors in Table 4 are too small. After Newey-West HAC correction (Table 5), the UV_{cum} standard error rises from 0.00402 to 0.00867 and its t-statistic changes from −55.85 to −25.89. Despite this, UV_{cum} remains highly significant (p < 0.001), and relative humidity retains significance ($t = 2.84$, p = 0.005). Temperature and wind speed were non-significant before and after correction. The primary degradation finding is unaltered: UV irradiance drives tensile strength loss, and the rate is 0.2245 MPa per MJ/m².

The WLS model with inverse-variance weights $w_i = \left(\mathrm{UV}_{\mathrm{cum},i} + 1\right)^{-0.6432}$ achieved weighted $R^2 = 0.9535$ (F(4, 506) = 2592.71, p < 0.001). The fitted WLS equation is:

$$\hat{\mathrm{TS}} = 239.863 - 0.2111 \cdot \mathrm{UV}_{\mathrm{cum}} + 0.0092 \cdot T + 0.0371 \cdot \mathrm{RH} + 0.1505 \cdot \mathrm{WS} \qquad (6)$$

The unweighted RMSE under WLS is 4.870 MPa, marginally above the OLS value of 4.715 MPa, which is expected: WLS minimizes weighted residual variance and trades a small increase in raw prediction error for substantially improved inference in the high-variance region. The UV coefficient is stable at −0.2245 (OLS) versus −0.2111 (WLS), confirming the rate of UV-driven degradation is consistent across both estimators. Figure 2 shows the residual spread before and after WLS correction.

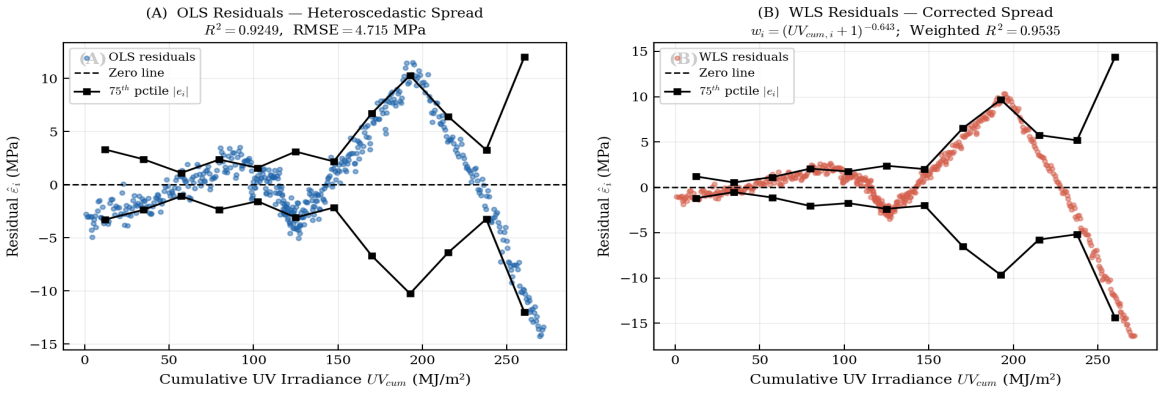

Figure 2. OLS vs. WLS residual comparison. Panel (A): growing spread under OLS. Panel (B): more uniform spread after WLS correction ($w_i = \left(\mathrm{UV}_{\mathrm{cum},i} + 1\right)^{-0.6432}$). Weighted R^2 improves from 0.9249 to 0.9535.

4.4. Second-Order Polynomial Regression Results

The polynomial model achieved R^2 = 0.9686 (adjusted R^2 = 0.9681, RMSE = 3.033 MPa; F(9, 501) = 1718.28, p < 0.001), a 35.4% reduction in prediction error relative to OLS. Table 6 presents all ten model terms with HAC-corrected standard errors. After HAC correction, six terms are significant at α = 0.05: UV, UV^2, T^2, RH^2, UV × RH, and T × RH. The UV × Temperature interaction, which appeared significant under OLS standard errors (t = −3.80, p < 0.001), does not survive HAC correction (t = −1.56, p = 0.119), a direct illustration of how serial autocorrelation inflates inferential confidence. Figure 3 shows contour plots for the two HAC-significant interactions.

Table 6. Polynomial regression coefficient estimates with newey-west HAC standard errors (R^2 = 0.9686, RMSE = 3.033 MPa; F (9, 501) = 1718.28; DW = 0.231, ρ_1 = 0.884).

Term	Coefficient	HAC Std Error	t (HAC)	p (HAC)	Sig.
Intercept	234.064	7.210	32.39	<0.001	***
UV (MJ/m²)	−0.1434	0.04875	−2.94	0.003	**
Temperature (˚C)	−0.2865	0.16904	−1.70	0.091	ns†
Rel. Humidity (%)	+0.2292	0.17660	1.30	0.195	ns†
UV^2	−0.000580	0.000113	−5.11	<0.001	***
Temperature^2	−0.01178	0.002780	−4.24	<0.001	***
RH^2	−0.003360	0.001140	−2.95	0.003	**
UV × Temperature	−0.001590	0.001020	−1.56	0.119	ns‡
UV × Rel. Humidity	+0.001450	0.000440	3.34	<0.001	***
Temperature × RH	+0.01172	0.001730	6.80	<0.001	***

***p < 0.001; **p < 0.01; ns = not significant after HAC. † Linear T and RH main effects retained under effect-heredity principle (their quadratic and interaction terms are significant). ‡ UV × Temperature was significant under OLS SEs (t = −3.80, p < 0.001) but loses significance after Newey-West HAC correction (p = 0.119). Coefficient estimates are unbiased; only SEs and derived statistics differ from OLS.

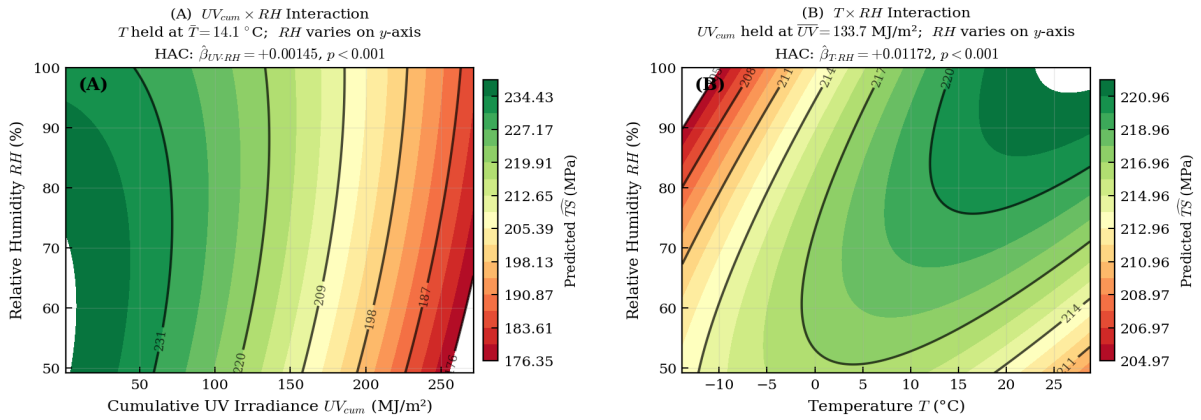

Figure 3. Second-order polynomial regression fitted-value contour plots. Panel (A): $UV_{cum} \times RH$ interaction (T held at mean = 14.1˚C; RH held at mean = 78.9% on y-axis). Panel (B): Temperature × RH interaction (UV_{cum} held at mean = 133.7 MJ/m²). Both interactions remain significant after Newey-West HAC correction. Green = higher predicted tensile strength (MPa); red = greater predicted degradation. $R^2 = 0.9686$, RMSE = 3.033 MPa.

4.5. Reliability Analysis: Weibull vs. Lognormal

Maximum likelihood fitting returned Weibull parameters of $\beta = 15.87$ and $\eta = 222.56$ MPa, and lognormal parameters of $\mu = 5.368$ and $\sigma = 0.083$. A shape parameter of 15.87 places the failure mode firmly in the wear-out regime, consistent with the accelerating UV^2 effect confirmed in the polynomial model. The Weibull distribution outperformed the lognormal on all three selection criteria: AIC (4290.85 vs. 4394.23; ΔAIC = 103.38), BIC (4299.32 vs. 4402.71), and KS statistic (0.1453 vs. 0.2207). Model selection results are in **Table 7** and probability plots in **Figure 4**.

Both KS statistics exceed the standard threshold of 0.060 and the Li [18] modified critical value of approximately 0.040 for estimated parameters, meaning neither distribution achieves a perfect absolute fit. The 511 observations form a single serially autocorrelated time series (DW = 0.038; $\rho_1 = 0.981$); distribution fitting by maximum likelihood assumes independence, so the reported AIC, BIC, and KS values should be interpreted as comparative indicators rather than exact information-theoretic quantities. The relative superiority of Weibull is nevertheless unambiguous: a ΔAIC of 103.38 over the lognormal is decisive under any reasonable adjustment, and the Weibull is the correct distributional choice for this material and dataset.

The B_{10} threshold, the 10th percentile of the fitted Weibull distribution, is 193.14 MPa, corresponding to a 20.2% reduction from the initial tensile strength of 241.93 MPa. Inverting the OLS regression equation (Equation (5)) with T, RH, and WS held at their dataset means, this B_{10} strength level is reached at approximately 231.3 MJ/m² of cumulative UV, or roughly 15.4 years at a reference UV accumulation rate of 15 MJ/m²/year [4]. Planners may use this as a maintenance planning threshold: the population-mean predicted tensile strength of the PPE backsheet reaches the B_{10} level at approximately year 15 under temperate mid-latitude conditions.

Table 7. Reliability Distribution Model Comparison ($n = 511$).

Distribution	Parameters	AIC	BIC	KS Stat.	Verdict
Weibull	$\beta = 15.87$, $\eta = 222.56$ MPa	4290.85	4299.32	0.1453	Best fit
Lognormal	$\mu = 5.368$, $\sigma = 0.083$	4394.23	4402.71	0.2207	

KS standard critical value (known parameters, $n = 511$, $\alpha = 0.05$): ≈0.060. Modified critical value for estimated parameters [18]: ≈0.040. Neither distribution achieves a perfect KS-based fit; model selection rests on AIC/BIC (ΔAIC = 103.38, decisive). AIC/BIC values are indicative given serially dependent observations; the Weibull advantage is robust under any reasonable autocorrelation adjustment.

Both KS statistics exceed the Stephens (1974) modified critical value (≈0.040); model selection based on AIC/BIC (ΔAIC = 103.38, decisive)

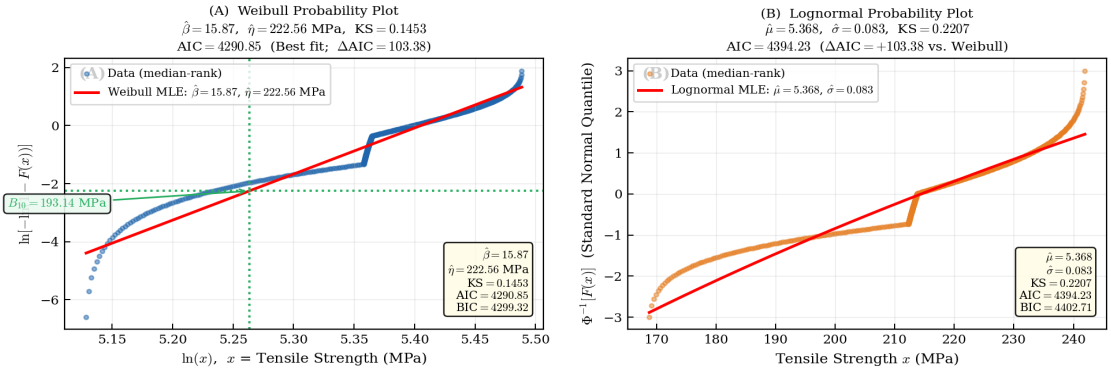

Figure 4. Weibull and lognormal probability plots (median-rank positions). Panel (A): Weibull fit ($\beta = 15.87$, $\eta = 222.56$ MPa, KS = 0.1453). Panel (B): Lognormal fit ($\mu = 5.368$, $\sigma = 0.083$, KS = 0.2207). Weibull is decisively superior (ΔAIC = 103.38). Both KS statistics exceed the Li [18] modified critical value; see **Table 7** footnote.

4.6. Cost-Benefit Analysis

Setting the standard PPE replacement cycle at 15.4 years from the Weibull B_{10} result, the NPV of the $92 field replacement cost discounted at 6% is $37.55 per module, giving the standard strategy a total NPV of $62.55. The premium fluoropolymer strategy, with no replacement event within the 25-year design life, has a total NPV of $55.00. The premium strategy carries a $7.55 per module NPV advantage. **Table 8** provides the complete breakdown.

The break-even threshold is an undiscounted field replacement cost of approximately $74 per module. Since the current estimate of $92 sits $18 above that threshold, the premium strategy is financially justified across a meaningful range of cost uncertainty. At 50,000 to 500,000 modules per utility installation, the per-module advantage aggregates to between $375,000 and $3.75 million in avoided lifecycle costs per project.

Table 8. Cost-Benefit Analysis: NPV of Total Costs per Module over 25-Year Design Life.

Cost Component	Standard PPE	Premium Fluoropolymer
Initial backsheet cost ($/module)	$25.00	$55.00
Replacement cycle (years)	~15.4	None (25-yr life)

Continued

Field replacement cost (undiscounted)	$92.00	$0.00
Replacement cost NPV @ 6%, 15.4 yrs	$37.55	$0.00
Total NPV of costs ($/module)	**$62.55**	**$55.00**

Initial material costs: Ramasamy *et al.* [19] and IRENA [20]. Field replacement cost ($92/module): Wiser *et al.* [21]; includes backsheet material, de-mounting, relamination, reinstallation, and downtime. Discount rate 6% p.a.: IRENA [20]. Replacement cycle from Weibull B_{10} result. Break-even undiscounted replacement cost ≈ $74/module.

5. Discussion

The most important thing this dataset communicates is also the simplest: UV radiation is what breaks down this backsheet. At the bivariate level, cumulative UV explains 92.1% of tensile strength variance before any other stressor enters the picture. That figure comes from a single Pearson correlation, not from model complexity. UV absorption in PET drives Norrish Type I and Type II reactions at carbonyl ester bonds, releasing chain scission byproducts that progressively reduce the laminate's tensile capacity. The WPET outer layer bears the highest UV load and is the first to embrittle, as the channel cracking data in Lin *et al.* [3] showed directly. At high enough accumulated doses, this embrittlement works inward through the PET core.

The autocorrelation finding carries real inferential weight. A DW statistic of 0.038 and a lag-1 residual autocorrelation of 0.981 reflect the physical reality of the measurement design: a single specimen measured at 511 points along its degradation trajectory. Each observation inherits the specimen's current damage state from the one before it. OLS standard errors in this setting are too small, and the conventional t-statistics are inflated. After Newey-West HAC correction, UV_{cum} remains highly significant at $t = -25.89$, so the primary finding about degradation rate is unchanged. What does change is the UV × Temperature interaction: it appeared significant under OLS ($p < 0.001$) and lost significance after HAC correction ($p = 0.119$). Temperature effects in this dataset appear to operate through the quadratic T^2 term and through co-action with humidity, rather than through a direct multiplicative interaction with UV dose. That is a substantive finding about the mechanism, not a technical footnote.

The two polynomial interactions that survived HAC correction are physically interpretable. The positive UV × RH coefficient ($\beta = +0.00145$, $p < 0.001$) suggests that at the UV doses observed here, higher humidity is associated with marginally better tensile strength retention, plausibly because absorbed moisture plasticizes the PET surface layer and delays brittle crack propagation. Whether this reverses at higher UV levels, where hydrolytic chain scission would dominate, cannot be determined from this dataset. The positive $T \times$ RH coefficient ($\beta = +0.01172$, $p < 0.001$) suggests a partial compensating effect when both temperature and humidity are elevated simultaneously, possibly through moisture-driven suppression of thermally induced crystallization in amorphous PET domains.

The Weibull result is unambiguous. A ΔAIC of 103.38 over the lognormal is decisive by any accepted standard, and the shape parameter of 15.87 describes a physically coherent wear-out pattern. Neither distribution achieves a perfect absolute KS fit, but for a single-specimen degradation record with heterogeneous microcrack distributions, this is expected rather than surprising. The B_{10} threshold of 193.14 MPa at roughly 15.4 years translates directly into a maintenance planning horizon: the population-mean predicted tensile strength reaches this level at approximately 231.3 MJ/m^2 of cumulative UV under temperate mid-latitude conditions.

Economics reinforce this timeline. A $7.55 per module NPV advantage for premium fluoropolymer looks modest in isolation, but it holds across a wide range of cost because the break-even threshold is $74 per module and field labor costs alone typically exceed that [21]. The remaining analytical limitations worth flagging are the reliance on a single UV accumulation rate of 15 MJ/m^2/year; the use of a single-specimen dataset, which means material-to-material variability cannot be separated from temporal autocorrelation. Future work should build stochastic, location-specific irradiance projections into the analysis to convert the B_{10} result into a climate-adjusted service life distribution rather than a single point estimate and should extend the dataset to multiple specimens to address both limitations simultaneously.

6. Conclusions

Using 511 sequential field measurements from a multilayer PPE PV backsheet spanning 271.6 MJ/m^2 of cumulative UV exposure, this paper developed and validated a six-stage statistical framework for tensile strength degradation modeling. The key findings fall into three groups.

On the degradation physics: cumulative UV irradiance is the decisive driver, explaining 92.1% of tensile strength variance on its own ($r = -0.960$) and remaining the dominant predictor at $t = -25.89$ after full statistical correction. The OLS model predicted a 25.1% total tensile strength reduction, closely matching the 26.7% measured by Lin *et al.* [3] under comparable conditions. The second-order polynomial model reduced predictive error by 35.4% (RMSE from 4.715 to 3.033 MPa), and six nonlinear and interaction terms survived HAC correction: UV, UV^2, T^2, RH^2, UV × RH, and T × RH.

On statistical validity: significant heteroscedasticity (BP LM = 192.93, $p < 0.001$) and very strong serial autocorrelation (DW = 0.038, $\rho_1 = 0.981$) were both detected and corrected. WLS addressed heteroscedasticity and improved weighted R^2 to 0.9535. Newey-West HAC standard errors corrected all inferential tests. Coefficient estimates are unbiased and unchanged; the corrections affect only standard errors and test statistics derived. The UV × Temperature interaction, significant under OLS, lost significance after HAC correction and should not be over-interpreted.

On reliability and cost: Weibull fitting was decisively superior to lognormal

(ΔAIC = 103.38), returning $\beta = 15.87$ and a B_{10} tensile strength threshold of 193.14 MPa at approximately 15.4 years. Cost-benefit analysis demonstrated a $7.55 per module NPV advantage for premium fluoropolymer backsheets, with the premium strategy financially justified whenever undiscounted field replacement costs exceed roughly $74 per module.

The framework developed here, covering Pearson screening, OLS/WLS regression with Breusch-Pagan and Durbin-Watson diagnostics, Newey-West HAC correction, polynomial modeling, and Weibull reliability analysis, is directly transferable to other backsheet materials and degradation modes. Future work should extend the approach to multi-specimen datasets to separate material variability from temporal autocorrelation and should incorporate site-specific stochastic UV projections to generate climate-adjusted service life distributions.

Author Contributions

Conceptualization, J.M. and T.K.B.; methodology, J.M.; software, J.M.; validation, J.M. and T.K.B.; formal analysis, J.M.; investigation, J.M.; data curation, J.M.; writing—original draft preparation, J.M.; writing—review and editing, J.M. and T.K.B.; visualization, J.M.; supervision, T.K.B.; project administration, T.K.B. All authors have read and agreed to the published version of the manuscript.

Conflicts of Interest

The authors declare no conflicts of interest regarding the publication of this paper.

References

[1] Lyu, Y., Fairbrother, A., Gong, M., Kim, J.H., Gu, X., Kempe, M., *et al.* (2020) Impact of Environmental Variables on the Degradation of Photovoltaic Components and Perspectives for the Reliability Assessment Methodology. *Solar Energy*, **199**, 425-436. https://doi.org/10.1016/j.solener.2020.02.020

[2] Al Mahdi, H., Leahy, P.G., Alghoul, M. and Morrison, A.P. (2024) A Review of Photovoltaic Module Failure and Degradation Mechanisms: Causes and Detection Techniques. *Solar*, **4**, 43-82. https://doi.org/10.3390/solar4010003

[3] Lin, C., Lyu, Y., Yu, L. and Gu, X. (2016) Correlation between Mechanical and Chemical Degradation after Outdoor and Accelerated Laboratory Aging for Multilayer Photovoltaic Backsheets. *SPIE Proceedings*, 9938, 57-67. https://doi.org/10.1117/12.2238216

[4] Kempe, M.D., Lyu, Y., Kim, J.H., Felder, T. and Gu, X. (2021) Fragmentation of Photovoltaic Backsheets after Accelerated Weathering Exposure. *Solar Energy Materials and Solar Cells*, **226**, Article 111044. https://doi.org/10.1016/j.solmat.2021.111044

[5] Damo, U.M., Ozoegwu, C.G., Ogbonnaya, C. and Maduabuchi, C. (2023) Effects of Light, Heat and Relative Humidity on the Accelerated Testing of Photovoltaic Degradation Using Arrhenius Model. *Solar Energy*, **250**, 335-346. https://doi.org/10.1016/j.solener.2023.01.002

[6] Zhang, J., Feng, K., Diaham, S., Liao, Q., Zhou, X. and Putson, C. (2022) Lifetime Evaluation of Photovoltaic Polymeric Backsheets under Ultraviolet Radiation: From Chemical Properties to Mechanical Modeling. *ACS Omega*, **7**, 45609-45616.

https://doi.org/10.1021/acsomega.2c06424

[7] Mitterhofer, S., Kempe, M. and Gu, X. (2024) Evaluation of Surface Crack Formation in Photovoltaic Backsheets Using Fragmentation and Finite Element Simulations. *IEEE Journal of Photovoltaics*, **14**, 311-318. https://doi.org/10.1109/jphotov.2024.3356119

[8] Smith, S., Mitterhofer, S., Moffitt, S.L., Jhang, S., Watson, S.S., Sung, L., *et al.* (2023) Long-term Durability of Transparent Backsheets for Bifacial Photovoltaics: An In-Depth Degradation Analysis. *Solar Energy Materials and Solar Cells*, **256**, Article 112309. https://doi.org/10.1016/j.solmat.2023.112309

[9] Chen, H. and Chen, C. (2025) A Study of the Response Surface Methodology Model with Regression Analysis in Three Fields of Engineering. *Applied System Innovation*, **8**, Article 99. https://doi.org/10.3390/asi8040099

[10] Kumar, N.K. (2023) Autocorrelation and Heteroscedasticity in Regression Analysis. *Journal of Business and Social Sciences*, **5**, 9-20. https://doi.org/10.3126/jbss.v5i1.72442

[11] Li, Y., Peng, S., Li, Y. and Jiang, W. (2020) A Review of Condition-Based Maintenance: Its Prognostic and Operational Aspects. *Frontiers of Engineering Management*, **7**, 323-334. https://doi.org/10.1007/s42524-020-0121-5

[12] Shama, M.S., Alharthi, A.S., Almulhim, F.A., Gemeay, A.M., Meraou, M.A., Mustafa, M.S., *et al.* (2023) Modified Generalized Weibull Distribution: Theory and Applications. *Scientific Reports*, **13**, Article No. 12828. https://doi.org/10.1038/s41598-023-38942-9

[13] Markert, J., Ensslen, F., Rist, T., Beinert, A.J., Job, E., Hädrich, I., *et al.* (2024) Mechanical Stability of PV Modules. *PV-Symposium Proceedings*, **1**, 1-12. https://doi.org/10.52825/pv-symposium.v1i.1237

[14] Gaddam, S.K., Pothu, R. and Boddula, R. (2021) Advanced Polymer Encapsulates for Photovoltaic Devices—A Review. *Journal of Materiomics*, **7**, 920-928. https://doi.org/10.1016/j.jmat.2021.04.004

[15] Greene, W.H. (2020) Econometric Analysis. 8th Edition, Pearson. https://books.google.com/books?id=TbottAEACAAJ

[16] Tan, V., Dias, P.R., Chang, N. and Deng, R. (2022) Estimating the Lifetime of Solar Photovoltaic Modules in Australia. *Sustainability*, **14**, Article 5336. https://doi.org/10.3390/su14095336

[17] Nelson, W.B. (2021) Statistical Methods for Reliability Data, Second Edition. *Technometrics*, **63**, 437-440. https://doi.org/10.1080/00401706.2021.1945328

[18] Li, J. (2018) EDF Goodness-of-Fit Tests Based on Centre-Outward Ordering. *Journal of Nonparametric Statistics*, **30**, 973-989. https://doi.org/10.1080/10485252.2018.1508676

[19] Ramasamy, V., Feldman, D., Desai, J. and Margolis, R. (2021) U.S. Solar Photo-Voltaic System and Energy Storage Cost Benchmark: Q1 2021. National Renewable Energy Laboratory.

[20] International Renewable Energy Agency (IRENA) (2023) Renewable Power Generation Costs in 2022. https://www.irena.org/Publications/2023/Aug/Renewable-Power-Generation-Costs-in-2022

[21] Wiser, R., Bolinger, M. and Seel, J. (2020) Benchmarking Utility-Scale PV Operational Expenses and Project Lifetimes: Results from a Survey of U.S. Solar Industry Professionals. Lawrence Berkeley National Laboratory.

https://eta-publications.lbl.gov/sites/default/files/solar_life_and_opex_report.pdf

[22] Hameed, M.A., Kaaya, I., Al-Jbori, M., Matti, Q., Scheer, R. and Gottschalg, R. (2024) Analysis and Prediction of the Performance and Reliability of PV Modules Installed in Harsh Climates: Case Study Iraq. *Renewable Energy*, **228**, Article 120577. https://doi.org/10.1016/j.renene.2024.120577